

Supporting Information for

Albumin protein coronas render nanoparticles surface active: Consonant interactions at air-water and at lipid monolayer interfaces

Nasim Ganji¹ and Geoffrey D. Bothun^{1,*}

¹Department of Chemical Engineering, University of Rhode Island, 303 Fascitelli Engineering Building, 2 East Alumni Ave, Kingston, RI 02881, United States

*Corresponding author. Tel: +1-401-874-9518, E-mail: gbothun@uri.edu

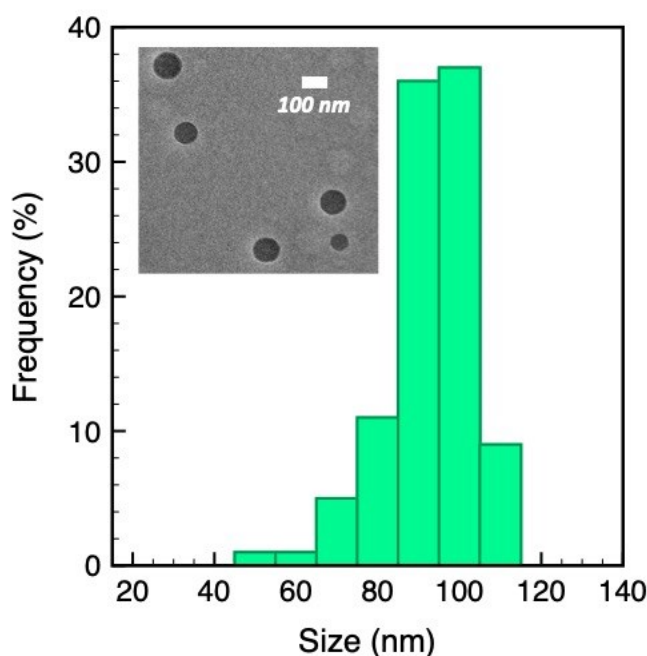


Figure S1. Histogram plot of PS NPs core diameter, d_c , based on TEM analysis (inset: a representative micrograph). The core diameter was determined by analyzing TEM images with the ImageJ software ($n > 50$).

Computational visualization of HSA. The atomic structure of HSA was based on crystal structure 1UOR in the Protein Data Bank. The online tool PROPKA was used to determine the protonation state of ionizable groups at pH 7.4. PDB2PQR was then used to determine the charge of each atom within the protein. (1) With the software Visual Molecular Dynamics, the 3-dimensional structure of HSA was rendered depicting the location of acidic (blue), basic (red), polar (yellow), and hydrophobic (silver) amino acid residues (Figure S2).

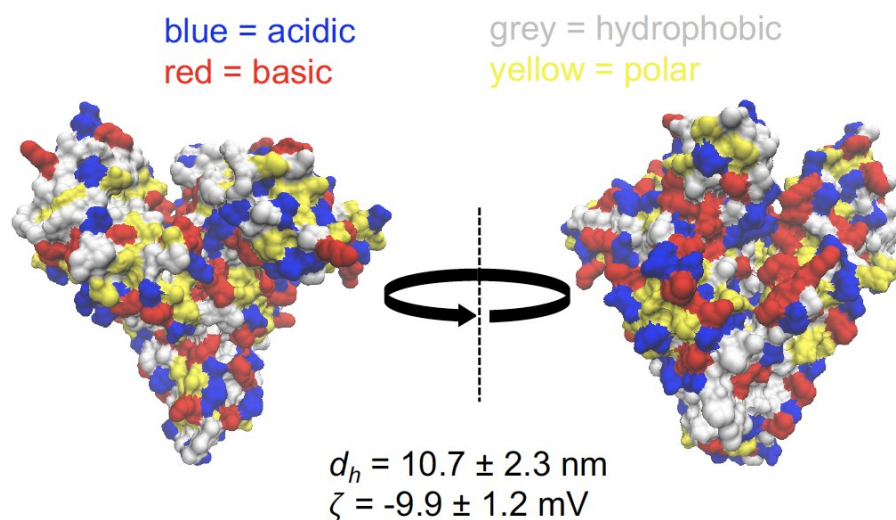


Figure S2. Computed structure of HSA at pH 7.4 depicting the location of acidic (blue), basic (red), polar (yellow), and hydrophobic (silver) amino acid residues. The hydrodynamic diameter (d_h) zeta potential (ζ) in pH 7.4 PBS are also shown. This image was made with VMD/NAMD/BioCoRE/JMV/other software support. VMD/NAMD/BioCoRE/JMV/ is developed with NIH support by the Theoretical and Computational Biophysics group at the Beckman Institute, University of Illinois at Urbana-Champaign.

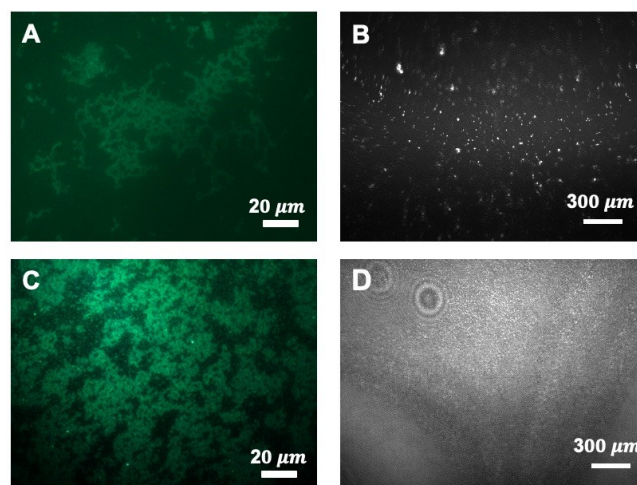


Figure S3. Representative fluorescence (A, C) and Brewster Angle (B, D) microscopy images of PS-NH nanoparticles (A, B) and PS-NH-HC complexes (C, D) at the air-water interface.

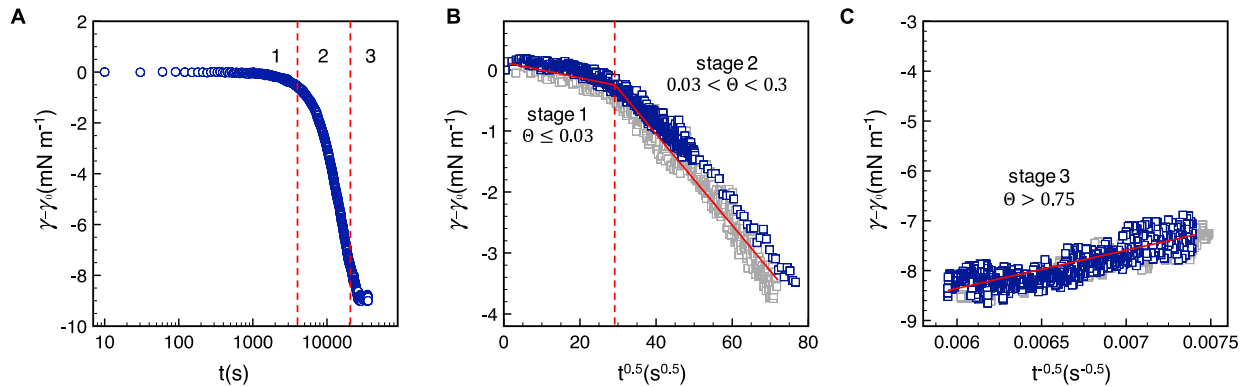


Figure S4. (A) Dynamic changes in interfacial tension, $\gamma - \gamma_0$, for PS-COOH-HC complexes, where three stages of behavior are displayed. In (B) $\gamma - \gamma_0$ is plotted as a function of $t^{0.5}$ at early times where the adsorption is diffusion-controlled; and in (C) as a function of $t^{-0.5}$, during the later stage of adsorption when it is barrier-controlled. Duplicate experiments are shown in (B) and (C) with grey and blue symbols. Dashed red lines denote the transition between stages and solid red lines represent linear line fits for each stage.

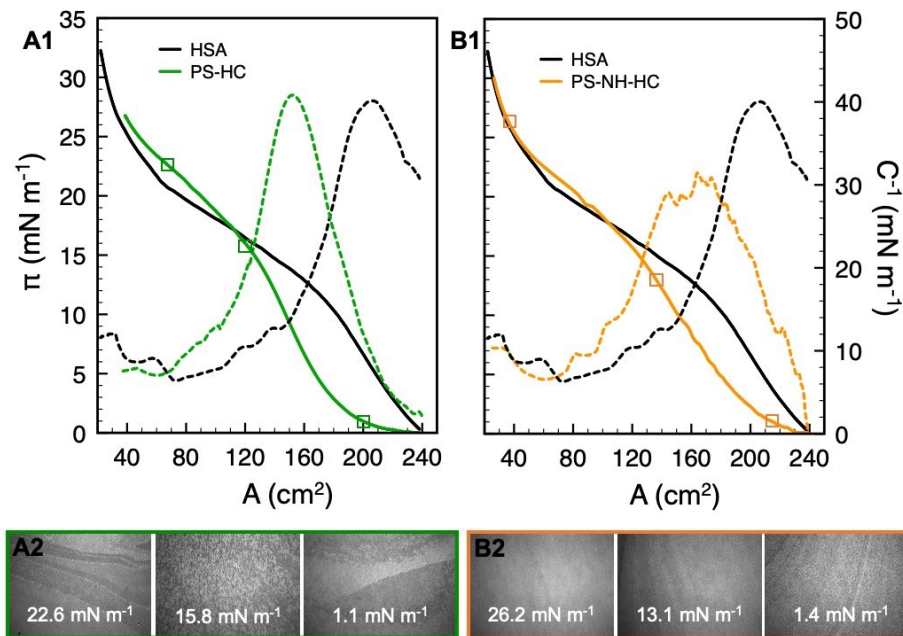


Figure S5. Surface pressure-area isotherms ($\pi - A$) and corresponding inverse compressibility moduli (C^{-1}) for HSA, (A1) PS-HC, and (B1) PS-NH-HC at the air-water interface. The open squares shown on the isotherms denote the conditions for BAM imaging shown in A2 and B2.

RBC monolayer morphology and $\pi - A$ isotherm. Surface pressure-area isotherm of the mixed lipid film mimicking the outer leaflet of human RBC membrane is shown in Figure S6A. Increasing π corresponded to a decrease in A with compression as the lipids packed more tightly

at the interface. There was a continuous phase transition from the gaseous (G)-phases at large lipid molecular area ($A \approx 113 \text{ \AA}^2 \text{ molecule}^{-1}$) to coexisting liquid-expanded (LE) and liquid-condensed (LC) phases at lower lipid molecular area where $\pi \geq 15 \text{ mN m}^{-1}$, with the monolayer collapse occurring at $\pi \approx 43 \text{ mN m}^{-1}$. The morphology of the film was visualized *in situ* using Brewster angle microscopy (BAM) technique. The BAM images were taken throughout the monolayer compression isotherm at $23 \text{ }^\circ\text{C}$. Representative fluorescence and Brewster angle microscopy images of the monolayers are shown in Figure S6B. The morphology of the films is comparable to that reported previously in the literature for the same lipid system.^(2–4) RBC monolayers existed as G phases at $\pi = 0.1 \text{ mN m}^{-1}$ and mixed of two LE phases at $\pi = 10 \text{ mN m}^{-1}$. First domains of LC phases appeared at $\pi = 15 \text{ mN m}^{-1}$. These domains existed up to the collapse point, while they enlarged with further compression and took a flower-like characteristic of pure SM monolayer.

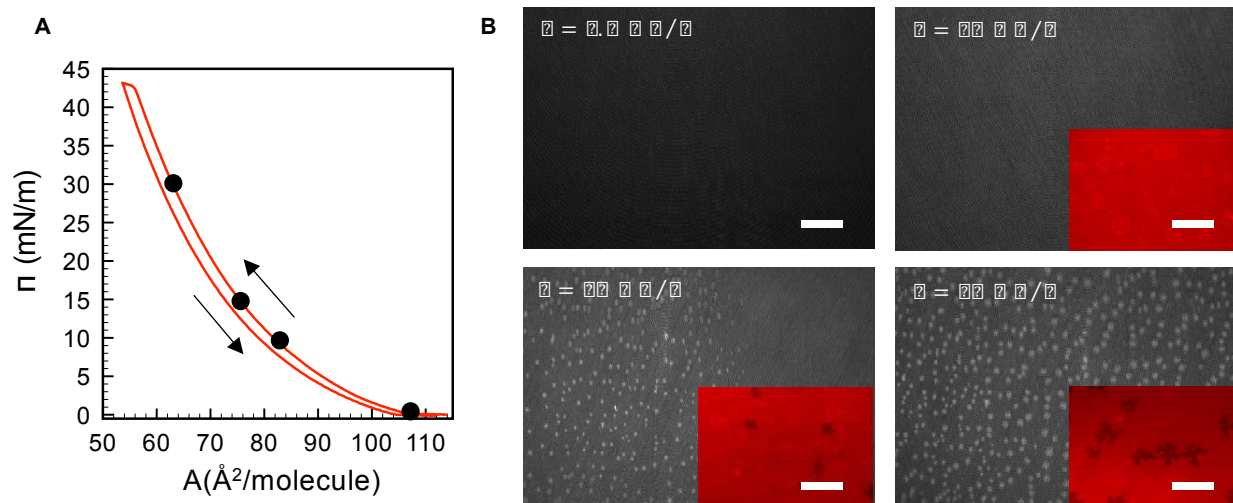


Figure S6. (A) Surface pressure-area (π - A) isotherm of the monolayer at the air-water interface at $23 \text{ }^\circ\text{C}$. Arrows indicate compression (solid line) followed by expansion (dashed line). (B) Representative fluorescence microscopy (Scale bars = $20 \text{ }\mu\text{m}$) and BAM images (Scale bars = $300 \text{ }\mu\text{m}$) of the film during a compression isotherm.

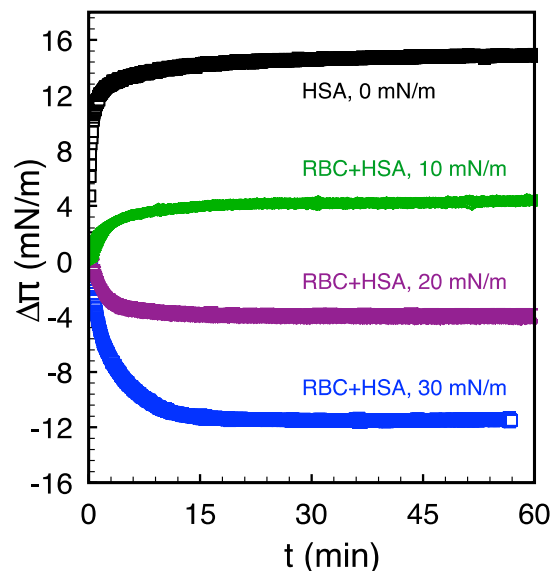


Figure S7. Change in surface pressure ($\Delta\pi$) during HSA adsorption to the air-water interface (0 mN/m) and to air-lipid-water interfaces formed with RBC outer leaflet lipids pre-compressed to surface pressures of 10, 20, or 30 mN/m.

REFERENCES

1. Dolinsky TJ, Nielsen JE, McCammon JA, Baker NA. An automated pipeline for the setup of Poisson-Boltzmann electrostatics calculations. *Nucleic Acids Res.* 2004; 32(suppl_2): W665-W667.
2. Haç-Wydro K, Dynarowicz-Łańska P. Externalization of phosphatidylserine from inner to outer layer may alter the effect of plant sterols on human erythrocyte membrane - The Langmuir monolayer studies. *Biochim Biophys Acta - Biomembr.* 2012; 1818(9): 2184–91.
3. Wydro P. The influence of cholesterol on multicomponent Langmuir monolayers imitating outer and inner leaflet of human erythrocyte membrane. *Colloids Surfaces B Biointerfaces.* 2013; 103: 67–74.
4. Arczewska M, Czernel G, Gagoś M. Effect of the amphotericin B and its copper complex on a model of the outer leaflet of human erythrocyte membrane. *J Phys Chem B.* 2016; 120(43): 11191–204.